

Multitask methods for predicting molecular properties from heterogeneous data

K. E. Fisher,¹ M. F. Herbst,^{2,3} and Y. M. Marzouk¹

¹*Department of Aeronautics and Astronautics, Massachusetts Institute of Technology*

²*Mathematics for Materials Modelling, Institute of Mathematics & Institute of Materials, École Polytechnique Fédérale de Lausanne, 1015 Lausanne, Switzerland*

³*National Centre for Computational Design and Discovery of Novel Materials (MARVEL), École Polytechnique Fédérale de Lausanne, 1015 Lausanne, Switzerland*

(*Electronic mail: kefisher@mit.edu)

(Dated: 1 February 2024)

Data generation remains a bottleneck in training surrogate models to predict molecular properties. We demonstrate that multitask Gaussian process regression overcomes this limitation by leveraging both expensive and cheap data sources. In particular, we consider training sets constructed from coupled-cluster (CC) and density function theory (DFT) data. We report that multitask surrogates can predict at CC level accuracy with a reduction to data generation cost by over an order of magnitude. Of note, our approach allows the training set to include DFT data generated by a heterogeneous mix of exchange-correlation functionals without imposing any artificial hierarchy on functional accuracy. More generally, the multitask framework can accommodate a wider range of training set structures—including full disparity between the different levels of fidelity—than existing kernel approaches based on Δ -learning, though we show that the accuracy of the two approaches can be similar. Consequently, multitask regression can be a tool for reducing data generation costs even further by opportunistically exploiting existing data sources.

I. INTRODUCTION

Predicting molecular properties based on first-principle approaches drives innovation across the physical sciences. However, exact prediction is infeasible due to the exponential scaling of the Schrödinger equation—the underlying quantum-mechanical description of materials systems. Decades of research have yielded numerous first-principle models to describe electronic structures approximately, each representing a compromise between computational cost and prediction accuracy. Coupled cluster (CC) methods are typical examples of high fidelity models which offer accuracy in exchange for considerable computational cost. Specifically, CCSD(T)—the “gold standard” of quantum-chemical prediction—suffers from a steep $O(N^7)$ scaling where N is the number of electrons in the target system.¹ In contrast, density-functional theory (DFT) methods are popular baseline models since they provide adequate accuracy for most systems while enjoying substantially lower cost (scaling only as $O(N^3)$).^{2–5}

Traditional workflows force users to settle on a single model which is cheap enough to result in manageable cost but still sufficiently high fidelity to give meaningful predictions. However, the advent of modern data-driven modeling has introduced new tools which make it possible to decouple expensive data generation from prediction. Statistical surrogates are trained with predictions from first-principle models and, once trained, can be substituted into workflows, making the prediction step considerably cheaper. In the context of building potential energy surfaces and interatomic potentials, these data-driven approaches have become the de facto standard.^{6–9} Simultaneously, large-scale data generation is facilitated by sophisticated workflow engines for high-throughput calculations^{10–12} and robust DFT methods inspired by mathematical research.^{5,13–16} The increasing amount of openly available data^{17–20} could in principle be readily employed, but qual-

ity is generally not homogeneous as each dataset’s author has made different modeling choices. Consequently, most surrogate models are single fidelity—all training data is generated using the same quantum-chemical method and the same numerical approach. Thus, heterogeneity has been an obstacle to opportunistically exploiting the already available data. With this work, we contribute to the promising development of multifidelity surrogates which do not require a single choice between accurate (but expensive) and fast (but crude) methods, but instead combine the advantages of both. Specifically, we consider multitask methods which construct a relationship between multiple regression problems without requiring precise information about the respective accuracy of each source.^{21,22}

Gaussian process (GP) regression is a popular tool for constructing surrogates informed by heterogeneous data. Several works^{23,24} have explored the use of multifidelity GP models²⁵ trained using two fidelities, namely a high and a low fidelity DFT approach. Alternatively, Δ -learning may be employed to model the difference between two levels of theory, then by adding that difference to low level predictions of the target to produce high level predictions.^{24,26,27} Though GP regression and the related technique of kernel ridge regression are common choices for fitting such models, in principle, any method of fitting a surrogate may be employed.^{24,27} Δ -learning can be extended to leverage more than two training data sets if multiple difference models are learned and summed.^{7,27} However, between each pair of training sets, data points must be in some way aligned to allow for learning a difference model. For example, in a model of the difference between DFT and CCSD(T), DFT predictions may only contribute to the training set if a corresponding CCSD(T) prediction is also available. Further, when either Δ -learning or multifidelity GP regression learn from more than two heterogeneous training sets, these sets must be assigned some order—for example, following a hierarchy in accuracy. Recent work²⁸ has pro-

posed an optimized linear combination of submodels as an alternative, but all coefficients in this linear combination must be re-optimized whenever any submodel is altered, and opportunistic data set construction is not fully explored.

Progress towards multifidelity approaches has also been made in the context of neural network surrogates. For example, transfer learning methods train an initial neural network on a larger source dataset, then re-optimize part of the parameters using a target dataset.^{6,29,30} For the prediction of atomistic properties, the source dataset might contain millions of DFT calculations while the target might be a smaller set of CCSD(T) predictions. In prior studies, it has been observed that transfer learning can produce higher accuracy than training a network on only one of these datasets.^{7,27} While the framework we discuss in this work is not restricted to GP regression strategies, we will focus exclusively on GP methods. In comparison to neural network approaches, where a rigorous mathematical explanation for the low generalization error of well-trained models is still lacking^{31,32}, GP approaches are more amenable to mathematical analysis.³³ This comparative transparency simplifies interpretation of the surrogate’s predictive process in the diverse training data configurations we analyze here. Additionally, GP methods have the advantage of yielding accurate predictions even for relatively small training set sizes. While the training cost of GP regression may become large as the size of the training set increases, many strategies for efficient scaling have been developed and can be routinely employed^{34–37}.

This work explores a GP regression approach which can accommodate an arbitrary number of quantum chemical datasets without an assumption of hierarchy. In particular, we employ the multitask framework²², which has been shown to easily incorporate heterogeneous data sources. The notion of heterogeneity in fact encompasses many possibilities. Fig. 1 compares the multitask method to other approaches by visualizing mappings between sets of molecules and the quantum chemistry methods which are used to generate viable training data sets. The highest level of theory used to construct these training sets will be called the primary level. In our case, the primary level will be CCSD(T). All other levels of theory will be categorized as secondary levels. Our secondary levels will include DFT methods using different density functional approximations (DFAs). Different levels of theory may contribute data points corresponding to the same set of molecules, different sets of molecules, or some union of shared and unique sets of molecules. Furthermore, the testing data set contains primary level predictions for target molecules. Thus, the multitask method has the option to use secondary predictions for the target molecules as part of the training set. The diagrams in Fig. 1 show several options for constructing a training set for inference. The impact of these choices on inference is under-explored in literature, and the multitask method is a useful tool for investigating the benefits of different training set configurations. Crucially, the multitask framework enables training with a “dataset of opportunity,” amalgamated from existing data sets, as an alternative to expending computational time to generate entirely new data.

A. Advantages of the Multitask Method

Our numerical experiments will demonstrate the following advantages of the multitask modeling approach. Key figures illustrating each claim are referenced in parentheses.

- Multitask models can achieve target accuracy with less computational cost than Gaussian process regression (Fig. 3).
- Accuracy of multitask inference improves as more DFT data is added to the training set. Furthermore, increasing the amount of training data from different secondary methods for the same molecule improves accuracy (Fig. 6).
- Unlike the Δ and multifidelity approaches, multitask methods can model more than two observation data sets without imposing an arbitrary order on the sets (Figs. 5 and 6)
- Multitask models have flexible training set requirements. The sets are constructed from multiple levels of theory, and the same molecules do not need to be included for each level (Fig. 3).

Flexibility is a key advantage of the multitask method compared to a single task or Δ -learning approach. The method is compatible with many training set structures. For instance, a multitask model can be trained with CCSD(T) data for one molecule set and DFT data for a different molecule set, with CCSD(T) and DFT data for the same molecule set, or with some in intermediary case. Models also have the option to train with DFT data for the molecules that we aim to make predictions for at the CCSD(T) level of accuracy. The flexible multitask framework makes it possible to explore the impact of different compositions of a training data set on inference as seen in Fig. 3. Consequently, we can determine the balance of expensive high level and cost effective low level data which best suits the problem setting and available data.

In Section II, we will review prediction with GP regression as well as the Δ and multifidelity methods before describing the multitask framework. Section III provides detail on our approach to testing different training set configurations, and Section IV describes our numerical tests. We demonstrate the performance of the multitask method on two examples: prediction of three-body energy of water trimer configurations and prediction of ionization potential of small organic molecules.

II. STATISTICAL MODELS

We review the formulation of Gaussian process regression models. Subsections II B through II D discuss variants of GP regression which leverage heterogeneous sets. See references^{21,22,25,33,38} for more detail.

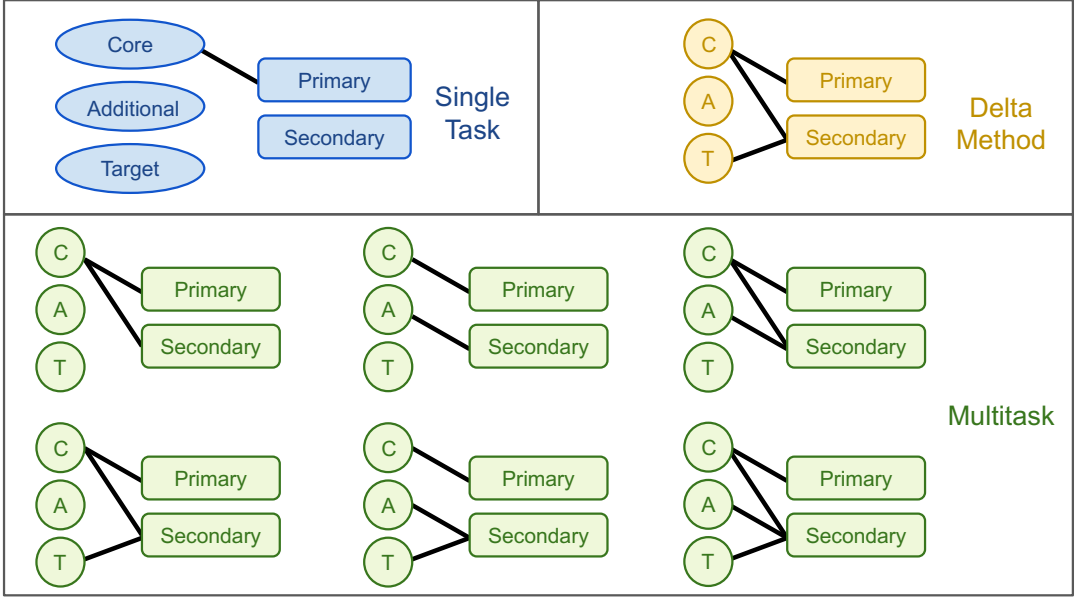


FIG. 1. Diagram of training data sets compatible with the methods considered in this work. Here, we define three sets of molecules—Core, Additional, and Target systems—and two quantum chemistry methods—primary and secondary. Our goal is to train a model that will predict our quantity of interest for the Target molecules with the accuracy of the primary method. By definition, the Core molecules are all systems for which we can compute training data with the primary method. Additional molecules are systems for which we have no primary data but which are not a part of the Target set. Theoretically, we may train using secondary predictions for molecules of all sets though not all inference methods support use of all data sets. The diagram shows the combinations of data sets and quantum chemistry methods supported by each inference method.

A. Gaussian Process Regression

Our goal is to predict values of some quantity of interest (QoI) f , given an identifying input feature \mathbf{X} . We train our predictive model using $\{\mathbf{X}_i, \mathbf{Y}_i\}_{i=1}^n$ where each \mathbf{Y}_i is a noisy observation of $f(\mathbf{X}_i)$. In our setting, we interpret imperfect first-principle predictions of the QoI as noisy observations of the true quantity. Each \mathbf{X}_i is some representation of the electronic structure of a molecular system. For our numerical results, we build \mathbf{X}_i using the well established Smooth Overlap of Atomic Potentials (SOAP).^{39–41} \mathbf{Y}_i is the CCSD(T) or DFT prediction of the quantity of interest for the i^{th} molecular configuration.

We will assume that each observation is independently perturbed by additive noise which follows identical Gaussian distributions. The corresponding model is

$$\begin{aligned} \mathbf{Y}_i &= f(\mathbf{X}_i) + \varepsilon_i, \\ \varepsilon_i &\sim N(0, \sigma^2). \end{aligned} \quad (1)$$

Before inference, we choose a mean function, $\mu(\mathbf{X})$ to describe the expected value of $f(\mathbf{X})$ and a kernel function, $k(\cdot, \cdot)$, to encapsulate our assumptions about the relationship between $f(\mathbf{X}_i)$ and $f(\mathbf{X}_j)$. Typically, $k(\cdot, \cdot)$ will have hyperparameters that are selected through optimization, then fixed during inference.

We will employ a Gaussian process prior model for our regression function:

$$f(\mathbf{X}) \sim \text{GP}(\mu(\mathbf{X}), k(\mathbf{X}, \mathbf{X}')). \quad (2)$$

As a consequence of this prior assumption, any finite collection, $\{f(\mathbf{X}_1), \dots, f(\mathbf{X}_n)\}$, will follow a multivariate normal distribution with mean $\mu = \{\mu(\mathbf{X}_1), \dots, \mu(\mathbf{X}_n)\}$ and covariance matrix K with entries at row i and column j given by $k(\mathbf{X}_i, \mathbf{X}_j)$. We are interested in inferring the values the function takes on at target inputs, and we collect these values in the vector, \mathbf{f}_* . Using this notation, we write the joint distribution on the observations and targets for inference:

$$\begin{bmatrix} \mathbf{Y} \\ \mathbf{f}_* \end{bmatrix} \sim N\left(\begin{bmatrix} \mu \\ \mu_* \end{bmatrix}, \begin{bmatrix} K_{pp} + \sigma^2 I & K_{p*} \\ K_{p*}^T & K_{**} \end{bmatrix}\right). \quad (3)$$

where I is the identity matrix. The specific subscripts of each covariance matrix represent the features that the matrix compares: p corresponds to our primary training data and $*$ indicates the target set. We note that in this single-fidelity setting all training data is contained in the primary set, but this will no longer be the case when we consider surrogates informed by heterogeneous data.

The marginal distribution of \mathbf{Y} is the model evidence, and conditioning \mathbf{Y} on \mathbf{f}_* yields the likelihood. To obtain the posterior, we employ the well known formula for conditioning part of a multivariate Gaussian random variable on the rest,³³ finding that

$$\begin{aligned} \mathbf{f}_* | \mathbf{Y} &\sim N\left(\mu_* + K_{p*}^T (K_{pp} + \sigma^2 I)^{-1} (\mathbf{Y} - \mu), \right. \\ &\quad \left. K_{**} - K_{p*}^T (K_{pp} + \sigma^2 I)^{-1} K_{p*}\right). \end{aligned} \quad (4)$$

Eq. (4) gives the probability distribution of our target values,

conditioned on our observations. The mean of this distribution is a correction to our prior mean based on the deviations of the observations from that mean. The predicted covariance indicates how much our observations have reduced our uncertainty, provided our assumptions are reasonably aligned to reality.

B. Δ -Learning

Suppose that for each training input, we have data on our QoI from multiple sources. We thus seek an inference model that leverages $\{\mathbf{Y}_{ij}\}_{i=1, j=1}^{n, m}$, where we have data for molecular configurations $i = 1, \dots, n$ and methods $j = 1, \dots, m$. A simple “pooling” approach may put all observations into one vector and proceed with inference via Eq. (4). Then, \mathbf{Y}_{ij_1} and \mathbf{Y}_{ij_2} are interpreted as independent observations of the QoI, $f(\mathbf{X}_i)$, for molecular configuration \mathbf{X}_i . The distinct behavior of each quantum chemical method is treated as a perturbation of some mean value by a realization of the noise distribution. We seek instead a model where the distribution of each \mathbf{Y}_{ij} is sensitive to j . Ideally, we want to map differences in electronic structures methods to differences in their predictions.

Method-specific features could be a solution, but construction of such features is challenging. One approach involves appending a vector which indicates the method category to each feature. This strategy puts a large burden on covariance hyperparameter optimization since one set of hyperparameters must encode differences between molecular configurations and between quantum chemical methods. Alternatively, to characterize the qualitative difference between methods within the features, we would have to solve the very problem for which we are creating the features in the first place—for instance, we would need to reliably predict CCSD(T) performance given CCSD(T) and DFT data from training molecules as well as DFT data for target molecules. Instead, we use this subsection to discuss Δ -learning, which directly models the differences between the predictions of quantum chemistry methods.

Δ -learning performs Gaussian process regression to predict differences, Δ_i , between observations obtained with two different methods for a given \mathbf{X}_i . If we retain our assumption that noise follows an independent, identically distributed Gaussian distribution, we have the model

$$\begin{aligned} \mathbf{Y}_{ij_1} - \mathbf{Y}_{ij_2} &\equiv \Delta_i = f(\mathbf{X}_i) + \epsilon_i, \\ f &\sim \text{GP}(\boldsymbol{\mu}_\Delta, k_\Delta(\mathbf{X}, \mathbf{X}')). \end{aligned} \quad (5)$$

where j_1 and j_2 indicate two prediction methods. An application of Eq. (4) yields a distribution on the regression function for Δ . Suppose our ultimate interest is to predict \mathbf{Y} at \mathbf{X}_* . Within the Δ framework, we can supply an observation from one method, say \mathbf{Y}_{*j_2} , in order to make a prediction for the value from the other method:

$$\mathbf{Y}_{*j_1} \approx \Delta_i + \mathbf{Y}_{*j_2}.$$

Thus, Δ -learning is suited to settings where calculations by method j_1 are both more accurate and more time consuming than calculations that use j_2 .

Consider a case where we want to build a model from an existing data set which includes predictions from CCSD(T) and several DFT methods. If the predictions all correspond to the same set of molecules, Δ -learning models have the ability to leverage more of the data set than conventional GP regression models. Unfortunately, Δ -learning is not-applicable in cases where predictions by different methods correspond to *different* molecular configurations. To use a DFT prediction for a molecule \mathbf{X}_i to train a Δ model between CCSD(T) and DFT, we also require a CCSD(T) prediction for the same molecule. In the following subsections, we consider alternative approaches which model disparities in data sources and have the ability to use all available observations.

C. Multifidelity Method

As a first step toward considering statistical models which train on heterogeneous data, we describe the multifidelity data fusion model.²⁵ The multifidelity approach defines two regression functions: f_p , representing the predictions from some high fidelity model, and f_s , representing a low fidelity model.²⁵ We assume the relationships

$$\begin{aligned} \mathbf{Y}_{ip} &= f_p(\mathbf{X}_i) + \epsilon_{ip} \\ &= \rho f_s(\mathbf{X}_i) + \delta_{ps}(\mathbf{X}_i) + \epsilon_{ip}, \\ \mathbf{Y}_{is} &= f_s(\mathbf{X}_i) + \epsilon_{is}. \end{aligned} \quad (6)$$

The term δ_{ps} captures the difference between the high fidelity model and the low fidelity model, scaled by hyperparameter, ρ . This disparity is endowed with a Gaussian process prior, as is the low fidelity regression function, f_s . The correlation, ρ , will be optimized before inference. As before, we assume that the additive noise terms, ϵ_{ip} and ϵ_{is} , are independent and drawn from identical, centered Gaussian distributions. Now, suppose we want to predict our targets, \mathbf{f}_* , at the high fidelity level. We can determine that the joint distribution of our high and low fidelity observations and our targets has covariance

$$\Sigma = \begin{bmatrix} \rho^2 K_{pp}^s + K_{pp}^\delta + \sigma^2 I & \rho K_{ps}^s & \rho^2 K_{p*}^s + K_{p*}^\delta \\ \rho K_{sp}^s & K_{ss}^s + \sigma^2 I & \rho K_{s*}^s \\ \rho^2 K_{*p}^s + K_{*p}^\delta & \rho K_{*s}^s & \rho^2 K_{**}^s + K_{**}^\delta \end{bmatrix}. \quad (8)$$

where σ^2 is the variance of the noise distribution. The superscript of each covariance matrix, \mathbf{K} , indicates which Gaussian process prior corresponds to the kernel function used in its construction, and the subscripts indicate the pairs of features that are compared. Bayesian inference yields an analytical posterior distribution, analogous to Eq. (4).

D. Multitask Method

“Multitasking” refers to a category of methods which consider several Gaussian process regression tasks and assume some relationship between these tasks. As with Δ -learning

or multifidelity fusion, multitasking can allow us to incorporate a larger dataset into our inference problem without just pooling the data into one observation vector. For instance, we can define a regression problem trained on CCSD(T) data as well as one trained on each DFA we consider. By modeling correlation between regression functions, we can use the DFA regression tasks to support prediction in the CCSD(T) task.

We can apply multitask regression to problems with m tasks where, for each task $j \in \{1, \dots, m\}$, we have observational data $\mathbf{Y}_j \in \mathbb{R}^n$. In practice, the method can be generalized, so that observation sets of different sizes are used for different tasks. Symmetric variants of multitask modeling treat all tasks equally. For instance, we may assume that all the data are modeled by a single Gaussian process whose covariance kernel is the Kronecker product of one kernel which relates the tasks and another which models relationships between data from the same task.²¹

In many cases, however, the goal is to perform regression for a primary task, and all other tasks may be considered secondary tasks which provide data that may be useful in learning the primary task. For our own setting, CCSD(T) is a natural choice of data for the primary regression task because we would like to make predictions which match this method in accuracy. Each set of DFT predictions made using a different DFA could inform a secondary regression task which supports the primary task. Thus, we consider an asymmetrical model²² in which secondary tasks are related through the primary task.

Suppose $\mathbf{Y}_p \in \mathbb{R}^{n_p}$ is the observation data for the primary task and $\mathbf{Y}_{s_j} \in \mathbb{R}^{n_j}$ is the data for the s_j^{th} secondary task. As before, we assume that each task has its own regression function

$$\mathbf{Y}_{ip} = f_p(\mathbf{X}_i) + \epsilon_{ip}, \quad (9)$$

$$\mathbf{Y}_{is_j} = f_{s_j}(\mathbf{X}_i) + \epsilon_{is_j} \quad \forall j = 1, \dots, m. \quad (10)$$

where each noise term is drawn independently from a centered Gaussian distribution with variance σ^2 . We now model a shared structure in the regression functions based on the primary function:

$$f_{s_j}(\mathbf{X}_i) = \rho_{s_j} f_p(\mathbf{X}_i) + \delta_{s_j}(\mathbf{X}_i) \quad \forall j = 1, \dots, m. \quad (11)$$

The specific component, δ_{s_j} , of the secondary function serves to “explain away” behavior that is not captured by the shared component, f_p .²² Both the correlation parameter, ρ_{s_j} and the specific component aim to mitigate negative transfer—learning behavior from secondary tasks that is not representative of the primary task. We make the prior assumption that f_p and δ_{s_j} for $j = 1, \dots, m$ follow Gaussian process distributions, each with a mean and kernel function which we will specify.

As was the case in subsections IIA through IIC, the first step toward inference with the multitask method is to determine the joint distribution on observations and targets. Note that the specific component of each task is modeled as independent of the others. Then, the covariance between observations due to the specific component is a block matrix with zeros corresponding to the covariance of specific functions for different tasks. Call this block matrix \mathbf{K}^δ . Let \mathbf{R} be a diagonal

matrix with dimensions equal to the number of observations, and let each diagonal element be the correlation hyperparameter of the corresponding task. The covariance of the joint distribution is

$$\Sigma = \begin{bmatrix} K_{pp}^p + \sigma^2 I & K_{ps}^p \mathbf{R} & K_{p*}^p \\ \mathbf{R} K_{sp}^p & \mathbf{R} K_{ss}^p \mathbf{R} + K^\delta + \sigma^2 I & \mathbf{R} K_{s*}^p \\ K_{*p}^p & K_{*s}^p \mathbf{R} & K_{**}^p \end{bmatrix}. \quad (12)$$

The superscript p indicates that a matrix was created with the primary kernel, and the matrix subscripts indicate the features that are compared. Inference proceeds as described in Eq. (4).

E. Beyond Two Tasks

Asymmetric multitasking assumes a relationship between regression functions—given by Eq. (11)—which is structurally reminiscent of the multifidelity fusion model—Eq. (6). Both assume that the regression function of one dataset is related to the regression function of another by a scaling parameter, ρ , and an additive disparity function, δ .

For only one secondary model, s_1 , the relationships between the regression functions posited by both methods are mathematically equivalent. However, asymmetric multitasking diverges more significantly from the multifidelity method when more than two models are considered. In the multifidelity approach, model hierarchy is reflected in a nested relationship between the functions,

$$\begin{aligned} f_p(\mathbf{X}) &= \rho_{s_1} f_{s_1}(\mathbf{X}) + \delta_{s_1}(\mathbf{X}), \\ f_{s_1}(\mathbf{X}) &= \rho_{s_2} f_{s_2}(\mathbf{X}) + \delta_{s_2}(\mathbf{X}), \\ &\vdots \\ f_{s_{j-1}}(\mathbf{X}) &= \rho_{s_j} f_{s_j}(\mathbf{X}) + \delta_{s_j}(\mathbf{X}), \end{aligned}$$

whereas in the asymmetric approach, all functions share the same relationship to the primary function

$$\begin{aligned} f_{s_1}(\mathbf{X}) &= \rho_{s_1} f_p(\mathbf{X}) + \delta_{s_1}(\mathbf{X}), \\ &\vdots \\ f_{s_j}(\mathbf{X}) &= \rho_{s_j} f_p(\mathbf{X}) + \delta_{s_j}(\mathbf{X}). \end{aligned}$$

Thus, compared to multifidelity fusion, the asymmetric multitasking approach more naturally accommodates a reasonably large number of regression tasks and relates each closely to the primary task of interest. Multitasking also holds a similar advantage over Δ -learning. Before the notion of a difference can be imposed it is necessary to choose some order between the source data sets. Such an order may be arbitrary, for example, if our data sets are generated by multiple DFAs with similar structure. In Section III, we will describe different compositions of a training data set which the multitask framework allows us to test.

III. HETEROGENEOUS TRAINING DATA

In our numerical examples, we train inference models using data for multiple molecular configurations computed with multiple quantum chemistry methods. The multitask method leaves many questions about the particulars of the training data set up to the researcher. For instance, available data must be apportioned to different tasks. One of our goals is to demonstrate that by training with data from multiple quantum chemistry methods, we can construct an inference model with prediction accuracy comparable to CCSD(T) with less computational expense than if we trained a single task model on CCSD(T) alone. Thus, our CCSD(T) data is the primary target of our regression problem and a natural choice to inform the primary task. We let each secondary task correspond to a different DFA. Examples with one up to four secondary tasks will be considered.

Another decision to be made is whether the training data sets for different tasks should include the same molecular configurations. In other words, we must determine whether or not to train with predictions for the same quantity by different methods. If our target for inference is the CCSD(T) prediction of energy for a system of water molecules, we may also choose to include DFT predictions of this energy in the training set for a secondary task. The relative benefits of constructing training sets with different degrees of intersection between tasks is under-explored in literature. Our work seeks to understand the impact of training set design on model performance.

We consider a range of possible training set compositions here, and Fig. 2 provides two example diagrams of our system for distinguishing between different constructions. We assign the molecular configurations to three sub data sets—Core (C), Additional (A), and Target (T). Dots in the figure indicate when configurations are available at a given level of theory. Black indicates availability to the training set, and green indicates membership of the testing set. The C set contains all configurations for which CCSD(T) training data is available, the A set contains configurations for which we have DFT data but no CCSD(T) data, and the T set contains configurations that we use to test our model’s ability to reproduce CCSD(T) level accuracy.

In our numerical results, we always train models with the CCSD(T) data from the C set and consider various compositions of the secondary sets. All secondary tasks are highlighted in gray. We identify different training set compositions by the letters of the sets of molecule which are included in our secondary training data. For example, the top diagram in Fig. 2 shows an A training set because the only DFT predictions available to train the model come from the Additional set. By contrast, the lower diagram shows a CAT training set because dots are present in the slots for DFT predictions for Core, Additional, and Target molecular configurations.

Furthermore, the vertical alignment of dots indicate when some of the same molecular configurations are present in the training sets for multiple tasks. In the CAT example in Fig. 2, the dots indicate that the secondary tasks share 20% of the C and A sets while the rest of the molecules in these sets are assigned to only one task each. In Section IV, we will show

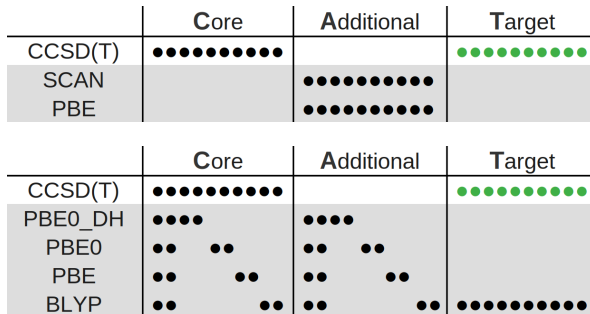


FIG. 2. Example data set structures. C, A, and T are sets of molecular configurations. C contains all configurations that the primary task, CCSD(T), is trained on. T contains the Target configurations; our goal is to estimate their properties with the accuracy of CCSD(T). The testing set is colored green. All secondary tasks are highlighted in gray. Configurations in set A can only be used for training secondary tasks. The vertical alignment of dots indicates that multiple tasks have access to the same molecular configurations.

results for the C, CT, A, AT, CA, and CAT training set configurations. Fig. 6 shows the impact of varying the fraction of molecules that the secondary tasks have in common.

Our testing framework is designed so that models trained with DFT Target data can readily be compared with equivalent models that do not train on this data. Since the inference model can make Target predictions one at a time, for each Target molecule we train a new model using the C set, A set, and the DFT prediction for only that Target molecule. While in practice we could take the much more efficient approach of training on the entire DFT Target set at once, our approach enables us to contrast each CAT model to a CA model with a training set which only differs by one molecule. Consequently, we can isolate the effect of the DFT level Target data on prediction performance.

In Section IV, we will examine the performance of the Δ and Multitask methods, informed by CCSD(T) and DFT predictions, and compare them to basic Gaussian process regression, informed only by CCSD(T).

IV. NUMERICAL EXAMPLES

A. Numerical Setup

We consider two case studies. In the first, the quantity of interest is the three-body (3-b) interaction energy of randomly selected water trimer configurations. The 3-b interaction term is isolated by subtraction of all 1-b and 2-b energies from the full energy of the trimer. We selected water because it is a simple molecule with unique properties which make it crucial for life and a popular subject for research.^{42–44} The second case study considers the prediction of the ionization potential of small organic molecules. Ionization potential is known to be challenging for DFT to capture accurately, so it is insightful to test the ability of inference models to predict this quantity.

1. Data Generation

For our first test case—inference of 3-b interaction energy—5986 water trimer configurations and corresponding CCSD(T) calculations were randomly selected from 45,332 configurations available from <https://github.com/jmbowma/q-AQUA>.⁴⁵ Density functional theory data was generated for 2992 of these configurations using Psi4.⁴⁶ We employed the PBE⁴⁷ and SCAN⁴⁸ functional approximations. The former was selected for its popularity in materials science research and the latter because its description of intermediate range dispersion has been found to contribute to accurate prediction of water energy differences.^{42,43} Following recent work on dispersion corrections,⁴⁹ we paired the PBE approximation with a D3 correction using finite damping and the SCAN approximation with a D3 correction using zero damping. Both DFT and CCSD(T) calculations employed a standard counterpoise correction to alleviate basis set superposition error.⁵⁰

The second test case is informed by the ionization potential of 3,165 molecular configurations, combinations of 479 different molecules and 7 configuration options.⁵¹ Configurations are subselected⁵² from the ANI-1 dataset²⁰ and contain only elements from the set $\{H, C, N, O\}$. We compute⁵³ ionization potential for these configurations using CCSD(T) as well as secondary tasks corresponding to data from four density functionals: PBE0_DH,⁵⁴ PBE0,⁵⁵ PBE,⁴⁷ and BLYP.⁵⁶

Quantification of cost in our numerical results refers to the cost of data set generation. The cost of inference is negligible next to quantum chemistry calculations. We base our cost model for each method on the average runtime of Psi4 computations for ten representative systems. For more details about the cost model, see Appendix A.

2. Features

We require features which can distinguish between molecular systems to serve as inputs, \mathbf{X}_i , to our Gaussian process models. Kernel functions use features to model the relationships between quantities of interest. As noted in Section II A, in our experiments we consider Smooth Overlap of Atomic Positions (SOAP) features, which have been successfully used to fit interatomic potentials in a Gaussian process based approach.³⁹⁻⁴¹ SOAP features are constructed based on the neighborhood of each atom in a system, so challenges arise when two systems contain different numbers of constituent atoms of elements. Multiple strategies have been proposed for constructing “global” features to capture entire systems.⁵⁷ The simplest approach is to take an average over the SOAP features for each atom in the system. Since this approach is computationally efficient and works well in practice, we apply it in our test cases. We chose SOAP parameters following experimentation and the advice of literature.^{58,59} More details are available in Appendices B and C.

3. Hyperparameter Optimization

Squared exponential kernels are used within all Gaussian process priors in our experiments.³⁸ These kernels introduce mean, variance (ν), and length scale (ℓ) hyperparameters in addition to the multitask correlation (ρ). We use the mean of our training data for each task as that task’s prior mean, calculated at training time. To estimate the remaining parameters, we construct an optimization data set containing 150 randomly selected molecular configurations which we subsequently exclude from our training and testing data sets. We assume here that we have access to predictions of our quantities of interest from each quantum chemistry method for each of these 150 molecular configurations, but when this assumption does not hold, a conventional GP regression model may be used to fill in missing data.

We estimate correlation parameters, ρ , using Pearson’s correlation coefficient between each secondary task optimization data set and the corresponding primary task data. Popular belief in literature holds that correlation parameters require a detailed optimization procedure,²⁷ but we find that these easy to obtain estimates work reasonably well in practice. A more detailed optimization is left for future work. We estimate $\ell \in \mathbb{R}$ by maximizing its log-marginal likelihood. This approach is easily extended to multifidelity and multitask cases by treating $Y_{ij} - \rho_j Y_{i1}$ as the i^{th} observation.⁶⁰ For the organic molecules example, we also use a maximum likelihood estimate for ν while for the water trimer example, we find better results from using an estimate of ν which minimizes mean absolute prediction error.

B. Three-Body Interaction Energy of Water Trimer

1. Multitask Performance

We first compare the performance of multitask models with only one secondary task to the performance of a traditional GP—or single task—model. Fig. 3 shows the error incurred by several implementations of each model when predicting the three-body (3-b) energy of water trimer configurations. We used the SCAN functional to generate the secondary task data, and Pearson’s correlation coefficient between the primary and secondary tasks is 0.997, indicating strong positive correlation. The three subplots of Fig. 3 cover six secondary training set configurations (C, CT, A, AT, CA, and CAT), labeled within the legends.

All models were tested on a Target set of 320 molecular configurations. We let the size of the Core set, N_c , take on values in $\{5, 10, 20, 40, 80, 160, 320\}$ for both inference methods and additionally consider $N_c \in \{640, 1280, 2560\}$ for the single task method. The subplots of Fig. 3 also show seven clear groupings of data points with steep slope. This effect is a consequence of the high cost of CCSD(T) relative to DFT. Each of the seven groupings corresponds to a different N_c . Given the size of the Core set, we let the number of configurations in the A set range from $0.5N_c$ to $6N_c$. Each point on the plot represents a model with a different training set size.

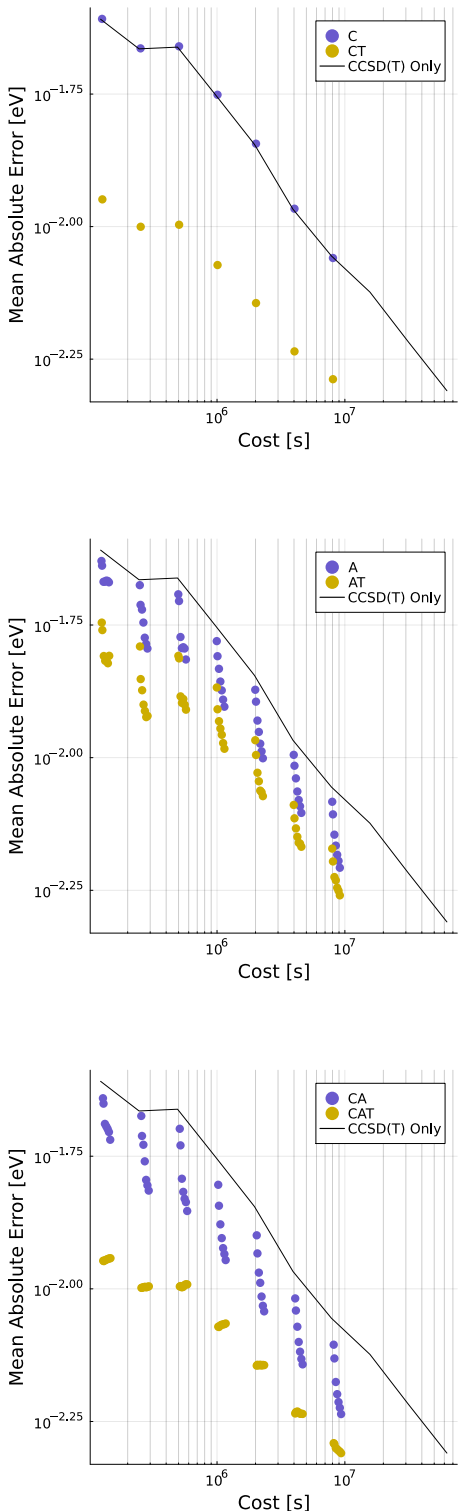


FIG. 3. **Water Trimer Case.** Comparison of the MAE of the multitask method for a range of training set constructions (scatter points) to the MAE of a GP regression model trained only with CCSD(T) data (black line). Predictions by the multitask method are informed by CCSD(T) and SCAN. The legends of the plots indicate the structure of the secondary training set according to the system presented by Fig. 2. All MAE reported are the average results obtained from six randomly chosen training sets.

The x axis indicates the cost of the training set while the y axis gives the average mean absolute error for six random assignments of molecular configurations to the C, A, and T sets. We provide details of our cost model in Appendix A.

For every training set configuration except C, the multitask method outperforms the single task reference, shown by a black line. Including T data from DFT in the training set leads to better results than corresponding cases without T in every example. In particular, training with secondary T data can enable the multitask method to exhibit an accuracy comparable to a GP model that is an order of magnitude more expensive.

While the C results demonstrate no significant improvement on the single task model, both A and CA results show steady improvement as the size of the A set increases. This behavior suggests that for the multitask method to be beneficial, secondary training data must cover molecular space that is not included in the CCSD(T) training data. We mention that it is possible that the behavior of C models would improve if we consider task dependent features or different relationships between task regression functions. We do not investigate these alternatives further here; instead, we focus on the usual setting where secondary DFT data for additional systems is cheap to obtain.

CT and CAT models are the best-performing multitask models, demonstrating very similar MAE per cost to each other. Furthermore, unlike the AT model, the CAT model does not show improvement as the size of the A set increases. It seems that for our setting, the combination of secondary C and T training data is so valuable to the model that any benefit from A data is dwarfed. We can hypothesize that when the model has access to data for the Core molecules from the primary and secondary tasks, it implicitly learns information about the difference between the tasks. Given secondary data on the Target, it can leverage the captured relationship between tasks to make an accurate prediction for the Target on the primary level.

Fig. 4 provides more insight to the relative roles of the training data sets and to the inherent flexibility of the multitask framework. While Fig. 3 demonstrates that multitask models can be successful when trained on many different training data configurations from the CAT framework, it does not directly compare the performance of the A and CA models. Such a comparison will illuminate the resilience of the multitask model to the loss of points in the training set which are common to primary and secondary tasks. We emphasize that this resilience is an advantage of the multitask method in comparison with Δ -learning—where no training is feasible without access to secondary C data. Each point on subplot (a) of Fig. 4 compares the average MAE of two multitask models: one with a CA secondary training set, the other with an identical A set but no secondary C data. As before, we are inferring the 3-b energy of water trimer configurations with only one secondary task. The closeness of the points to the reference $y = x$ line shows that there is minimal effect on accuracy when the secondary C data is excluded from the training set. In fact, the median improvement in accuracy from using the CA training model instead of an A training model is 0.0007 eV. By comparison, the median improvement in accu-

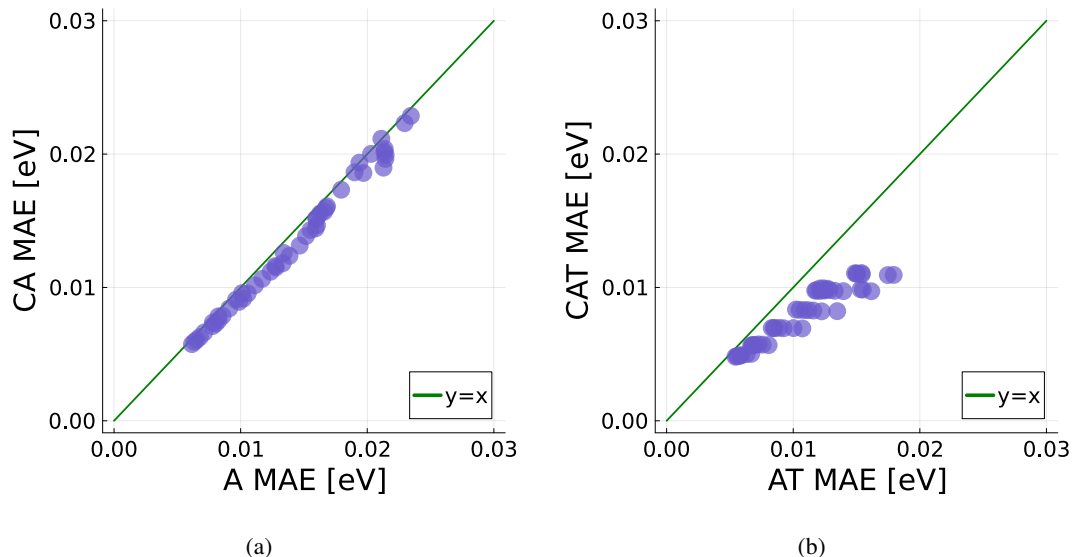


FIG. 4. **Water Trimer Case.** Effect of including Core and Additional data in secondary training sets. Each indigo point represents a comparison between two multitask models where one model uses a training set which is a subset of the other. In (a), this comparison is between A and CA training configurations, and in (b), we compare AT and CAT configurations. For each pair of models compared, both the primary training data and the secondary data from the A set are identical. The $y = x$ line is plotted in green for reference.

racy from combining DFT data from the A set with CCSD(T) training data—that is, switching from a single task approach to a multitask method trained on an A set—is 0.004 eV.

Subplot (b) of Fig. 4 also compares models trained with and without C secondary data in the case where all of these models also train on secondary Target data. While the AT models perform well, there is a penalty to losing access to secondary C training data when secondary Target data is also available. The median improvement in accuracy when switching from an AT model to a CAT model is 0.002 eV, a third of the 0.006 eV median improvement incurred from switching from a single task approach to an AT multitask model with the same CCSD(T) training cost. As we remarked previously, when the model trains on secondary C data, it likely gains information about the difference between the primary and secondary tasks. This information is most useful to the model when it also has access to secondary predictions for the Target molecules.

2. Comparison with Δ -learning

Δ -learning is trained on differences between predictions of our quantity of interest while the single and multitask methods are trained on absolute predictions of the quantity of interest. Table I reports summary statistics for these data sets. In this case, the mean and variance of the differences between quantum chemistry methods are smaller by at least an order of magnitude than those of any set of quantum chemistry predictions. Since Δ -learning is trained on differences to predict differences, it is expected that this method will produce smaller mean absolute error than a method trained on absolutes to predict absolutes.

By modifying our choice of tasks, we can design a multi-

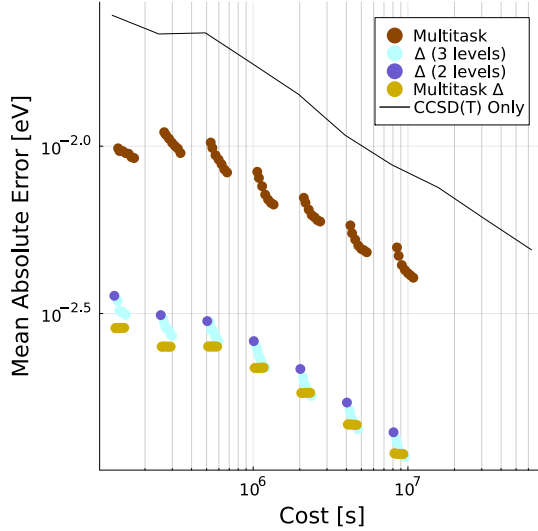
	CCSD(T) [eV]	SCAN [eV]	PBE [eV]
absolute mean	0.0205	0.0223	0.0225
absolute median	0.0126	0.0144	0.0155
variance	0.0009	0.0010	0.0011

	CCSD(T)–SCAN [eV]	CCSD(T)–PBE [eV]
absolute mean	0.0021	0.0037
absolute median	0.0013	0.0018
variance	1.1×10^{-5}	3.2×10^{-5}

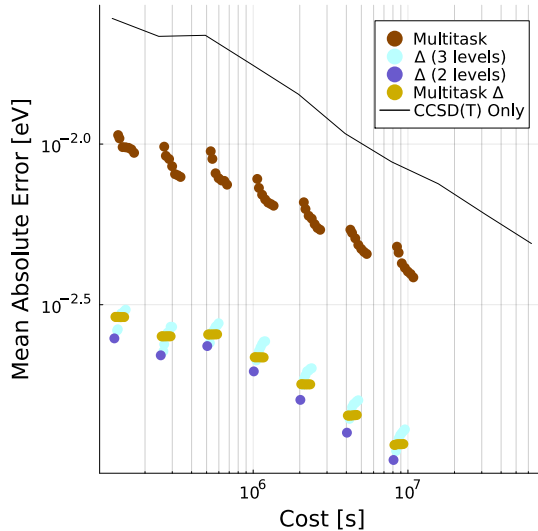
TABLE I. **Water Trimer case.** Summary statistics for absolute quantum chemistry predictions and for differences.

task model which trains on and predicts differences. We call this the multitask Δ option. Fig. 5 compares this option to the multitask method on absolutes as well Δ -learning. For each inference method, the average mean absolute error obtained for six random assignments of the training data is plotted for each of the same data set sizes which were considered in our previous experiments. The CAT secondary training set structure is used for the multitask absolute models as well as the multitask difference models. As expected, the multitask absolute model is not as successful as those which train on and learn differences.

In subplot (a) of Fig. 5, the object of estimation is the difference between CCSD(T) and PBE computations for each molecular system. For the multitask Δ option, we let the primary task be exactly this difference. The secondary task is the difference between SCAN and PBE computations which has correlation coefficient 0.782 with the primary task data. Re-



(a) Estimation of CCSD(T)-PBE



(b) Estimation of CCSD(T)-SCAN

FIG. 5. **Water Trimer Case.** The MAE of different inference methods: GP regression (line), multitask regression trained with a CAT secondary set (orange), two level Δ -learning (indigo), three level Δ -learning (light blue), and multitask inference on Δ s (gold). Reported performance is the average from six draws of each training set.

sults of the multitask Δ option are plotted in gold. The basic Δ -learning model is plotted in indigo and uses only two levels of theory, CCSD(T) and PBE, to predict their difference. Note that these models are the single task variant of the multitask Δ approach—they are trained only on the primary task. Therefore, Subplot (a) provides another example where the multitask method outperforms its single task counterpart, in this case with correlation parameter $\rho = 0.782$. The turquoise

points represent a Δ -learning model trained with three levels of theory: CCSD(T), SCAN, and PBE. This model is the sum of a pair of two level models where the top level of the first difference—between SCAN and PBE—is the bottom level of the second—between CCSD(T) and SCAN. Given sufficiently large training sets for the lower levels of theory, this method is comparable with the multitask Δ option. The multitask Δ option outperforms most other models, particularly when either C or A is relatively small.

Subplot (b) of Fig. 5 shows the performance of the same set of methods when the primary and secondary tasks demonstrate a slight negative correlation. In this case, the extra data from the secondary task does not contribute to improved inference of the primary task. Here, we estimate the difference between CCSD(T) and SCAN predictions. For all descriptions accompanying Subplot (a), we reverse the roles of SCAN and PBE for Subplot (b). The major difference between the cases is the correlation coefficient between data for CCSD(T)-SCAN and PBE-SCAN: $\rho = -0.271$. The multitask models shown in Subplot (b) demonstrate the limitations of choosing Pearson’s coefficient as the correlation parameter. The multitask Δ option and three level Δ -learning do not perform as well as two level Δ -learning in this setting. This behavior suggests that the multitask method requires a stronger correlation between tasks to outperform the single task method. Further, the subplot shows that the multitask Δ option outperforms three level Δ -learning for models trained on larger amounts of DFT data. Thus, three level Δ -learning seems to suffer more from problematic data than the Multitask Δ option. Importantly, Δ -learning has no correlation parameter and cannot adjust the contribution of each difference model. Though we have left a detailed optimization of the Multitask Δ option’s correlation parameter for future work, we observe that $\rho = 0$ can always be chosen. Therefore, the fully optimized multitask Δ option will always perform at least as well as two level Δ -learning. Consequently, the multitask framework makes it possible to benefit from useful secondary datasets which two level Δ -learning cannot accommodate while offering more protection against uncorrelated data than three level Δ models.

In practice, we may have more than two tasks available to support inference, so we can further contrast the methods discussed in this section by considering how they scale to more tasks. Suppose that alongside PBE and CCSD(T) we want to include n additional DFT functionals y_1, \dots, y_n . Then, Δ -learning requires us to put all quantum chemistry methods in some order—with CCSD(T) first and PBE last and the y_j in between. The difference between neighboring pairs of methods is then learned. However, hierarchies in DFA accuracy can be difficult to predict and differ between problem settings. This necessary ordering can thus become rather arbitrary. By contrast, the multitask Δ option would incorporate the n new secondary tasks based on the differences to PBE, i.e. $y_j - \text{PBE}$. Each of these secondary tasks can be directly related to the primary task through a correlation parameter—which thus eliminates the need to impose an arbitrary order.

C. Ionization Potential of Small Organic Molecules

	PBE0_DH	PBE0	PBE	BLYP
ρ	0.970	0.967	0.954	0.955

TABLE II. **Organic Molecules Case.** Pearson’s correlation coefficients between each secondary task and the primary task data set. The column headers give the DFA used to generate the secondary set.

We now turn our attention to the prediction of the ionization potential of small organic molecules made up of elements in $\{C, N, O, H\}$. Our secondary data for this example includes up to four tasks, generated with the PBE, PBE0, PBE_DH, and BLYP functionals, respectively. Table II shows the correlation parameter used to relate each of these secondary tasks to the primary task data, generated with CCSD(T). As in the water trimer example, we consider Core sets of sizes $\{5, 10, 20, 40, 80, 160, 320\}$. The Target set contains 320 molecular configurations. We let the number of molecules in the A set range from 1 to 6 times the number of molecules in the C set. As Section III visualizes, once the C and A sets have been fixed, there is still a design choice in allotting the molecular configurations to secondary tasks. We consider three cases: (1) the molecules in both C and A are randomly distributed among tasks, so no two tasks have access to training data for the same molecule, (2) half of the molecules in these sets are common to all tasks while the other half are distributed among the tasks with no redundancy, and (3) all tasks have access to training data for all molecules in both C and A. These cases correspond—in order, from the top down—to the three rows of Fig. 6.

In Fig. 6, as for previous results, the reported mean absolute error is the average over six tests produced by randomly assigning molecules to the C, A, and T sets. The left column of subplots compares results for multitask models trained on CA data sets to single task models trained only on CCSD(T) while the right column considers multitask models trained on CAT data. Translucent stripes encompass the results for models with different total numbers of tasks. For the two task case, the secondary task data is generated with PBE, and for the three task case the secondary data comes from PBE and PBE0. In all cases, secondary Target data is only generated with PBE. Recall that in our testing framework, when we train with the T data set, we train a custom model for each Target molecule. Specifically, the only T molecule in the training set is the molecule which we will use the model to predict. We remark that in practice it would not be necessary to train a new model for each molecule in the Target set.

As we observed in the water trimer case, the multitask models consistently perform better than single task models of comparable cost. Especially for relatively small training sets, the multitask method shows an improvement in performance when secondary Target data is included in the training set. Fig. 6 also informs us about the utility of including more than one secondary task in a model. Note that for each number of tasks we consider, we implement models with the

same combinations of C, A, and T set sizes. In the top row, molecules in the C and A sets are each assigned to exactly one secondary task, regardless of the total number of secondary tasks. Therefore, in this row, for each model implemented with two total tasks, we consider models of the same cost implemented with three tasks and with five tasks. The results show that for sufficiently large training sets, there is a benefit to training with multiple tasks for a given budget. For smaller datasets, two tasks may lead to performance as good or better than a larger number of tasks. In particular, the top subplot in column (b) suggests that two task models perform particularly well when given a relatively inexpensive training set of the CAT structure. Note that, in each model, only one secondary task is given access to T data. Thus, in this setting, the decrease in performance when new tasks are added likely comes from siphoning off part of the computational budget to train tasks which do not have access to T data.

We can also consider whether it is useful to train on more than two predictions for the same molecular configuration. The middle row of Fig. 6 shows cases where each task has access to training data for the same 50% of molecules in the C set as well as 50% of the molecules in the A set while the remaining molecules are distributed one per task, and the final row shows cases where all tasks have access to all data in the C and A sets. From these subplots, we conclude that there is a benefit to training our model on multiple secondary predictions for the same molecule.

V. CONCLUSION

The present work has demonstrated that inference models see a general benefit from leveraging all available data. Furthermore, use of the multitask framework can reduce the cost of generating entirely new training data by an order of magnitude and can also facilitate the opportunistic incorporation of existing datasets of heterogeneous quality into the training set. Our work is the first to explore a multitask GP regression model in a materials science setting. Significantly, the multitask framework is not restricted to the choice of GP inference, and future work can investigate training models with neural networks and other tools for regression.

Unlike other machine learning methods for constructing surrogates from ab initio data, the multitask model does not require all data sources be ordered in a hierarchy of accuracy. In this work, the data which informed our primary task—generated with CCSD(T)—was the most accurate in our training set, but we were also able to leverage an arbitrary number of secondary data sets without any information on their accuracy relative to each other. This feature of the multitask method is particularly useful when employing datasets constructed from different density functional approximations. We found that multitask model performance improves as we increase the number of secondary sets in the training data which include predictions for a molecule of interest. The influence of each secondary dataset is controlled by a correlation parameter, and we found that in most settings an estimate of Pearson’s correlation coefficient from training data works well. Use of

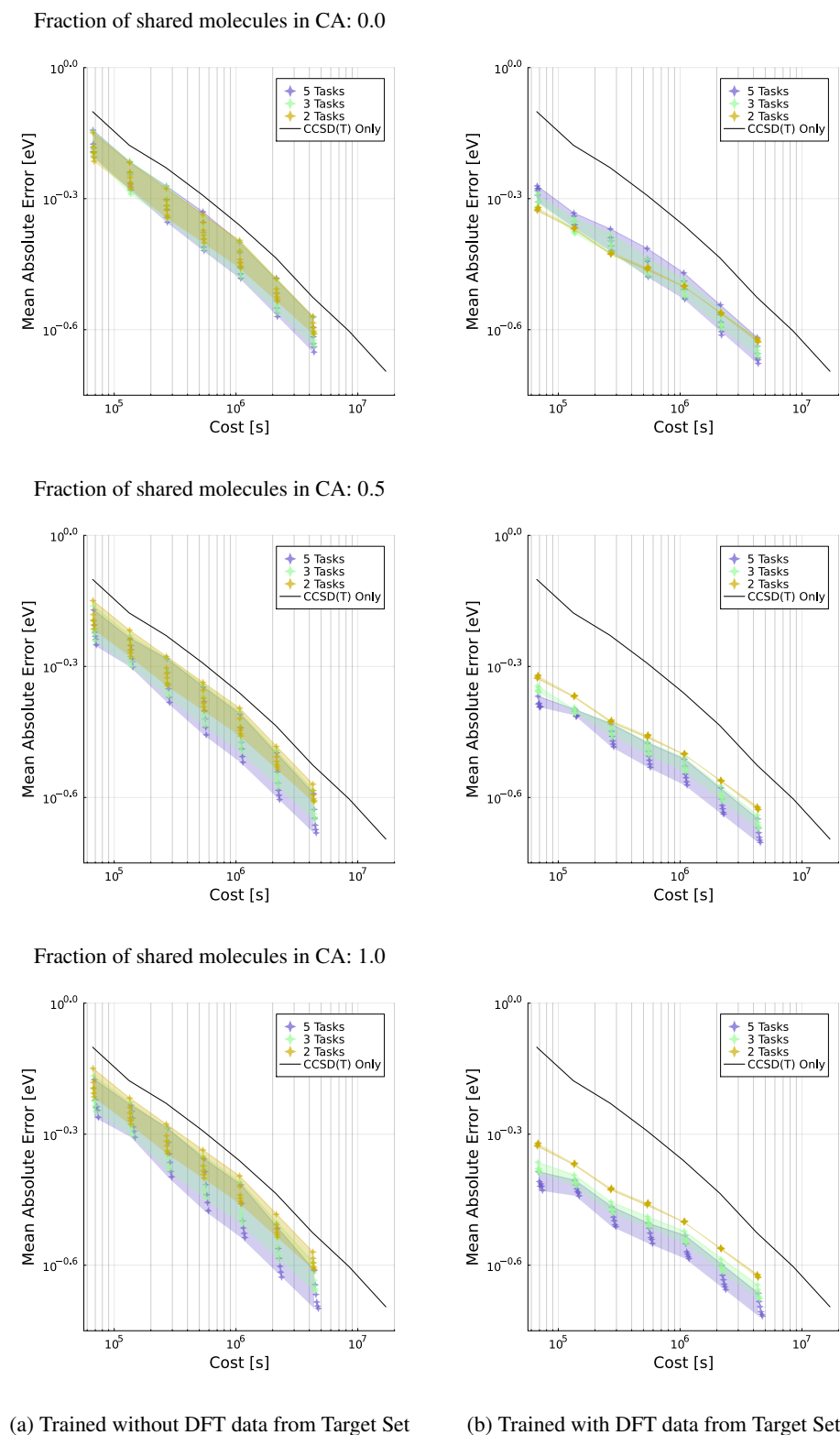


FIG. 6. **Organic Molecules Case.** For different numbers of tasks (indicated by color), plots show MAE versus cost. Note that $10^{-0.3}$ eV is approximately half an electronvolt. For each row, a given fraction of all molecules in the C and A sets are used to generate training data for all secondary levels, and the remaining molecules are split among the secondary levels. The fractions are given at the top of each row. Models represented in column (a) were trained without DFT data from the T set while models in column (b) had access to this data.

this estimate simplifies implementation of the method. The multitask method also supports training on differences, and with appropriate choice of correlation parameter, multitask difference models can perform at least as well as and often better than Δ models. To explore the framework's flexibility, we demonstrated the success of the multitask method on diverse training data set configurations.

ACKNOWLEDGMENTS

The authors would like to thank Yeongsu Cho, Chenru Duan, Dallas Foster, and Heather Kulik for insightful discussions. MIT SuperCloud and Lincoln Laboratory Supercomputing Center are acknowledged for providing the HPC resources that have contributed to the research results reported within this paper.⁶¹ This material is based upon work supported by the Department of Energy, National Nuclear Security Administration PSAAP-III program, under Award Number DE-NA0003965 as well as work supported by the National Science Foundation Graduate Research Fellowship under Grant No. 1745302. This research was supported by the NCCR MARVEL, a National Centre of Competence in Research, funded by the Swiss National Science Foundation (grant number 205602).

AUTHOR CONTRIBUTIONS STATEMENT

Katharine Fisher: Conceptualization (equal); Data Curation (equal); Methodology (equal); Software (lead); Writing – original draft (lead); Writing – review and editing (equal); Visualization (equal). **Michael Herbst:** Conceptualization (equal); Data Curation (equal); Methodology (equal); Supervision (equal); Writing – review and editing (equal); Visualization (equal). **Youssef Marzouk:** Conceptualization (equal); Methodology (equal); Supervision (equal); Writing – review and editing (equal); Visualization (equal).

CONFLICT OF INTEREST STATEMENT

The authors have no conflicts to disclose.

DATA AVAILABILITY STATEMENT

All data supporting this work are openly available. All code to reproduce figures as well as all DFT predictions for the three-body energy of water trimers can be found at <https://doi.org/10.5281/zenodo.10387647> or https://github.com/kefisher98/Multitask_GP/tree/Multitask. Water trimer configurations and CCSD(T) predictions for three-body energy are available at <https://github.com/jmbowma/q-AQUA>. The data that support the findings of this study for the small organic molecules example are at <https://doi.org/10.5281/zenodo.10215421>.

- ¹M. E. Harding, T. Metzroth, J. Gauss, and A. A. Auer, "Parallel calculation of ccsd and ccsd(t) analytic first and second derivatives," *Journal of Chemical Theory and Computation* **4**, 64–74 (2008).
- ²L. Ying, J. Yu, and L. Ying, "Numerical methods for kohn–sham density functional theory," *Acta Numerica* **28**, 405–539 (2019).
- ³J. Perdew and K. Schmidt, "Jacob's ladder of density functional approximations for the exchange-correlation energy," in *AIP Conference Proceedings* (2001) presented at AIP Conference Proceedings 577.
- ⁴L. Goerigk and S. Grimme, "A thorough benchmark of density functional methods for general main group thermochemistry, kinetics, and noncovalent interactions," *Physical Chemistry Chemical Physics* **13**, 6670–6688 (2011).
- ⁵A. M. Teale, T. Helgaker, A. Savin, C. Adano, B. Aradi, A. V. Arbuznikov, P. Ayers, E. J. Baerends, V. Barone, P. Calaminici, E. Cancès, E. A. Carter, P. K. Chattaraj, H. Chermette, I. Ciofini, T. D. Crawford, F. De Proft, J. Dobson, C. Draxl, T. Frauenheim, E. Fromager, P. Fuentealba, L. Gagliardi, G. Galli, J. Gao, P. Geerlings, N. Gidopoulos, P. M. W. Gill, P. Gori-Giorgi, A. Görling, T. Gould, S. Grimme, O. Gritsenko, H. J. A. Jensen, E. R. Johnson, R. O. Jones, M. Kaupp, A. Koster, L. Kronik, A. I. Krylov, S. Kvaal, A. Laestadius, M. P. Levy, M. Lewin, S. Liu, P.-F. Loos, N. T. Maitra, F. Neese, J. Perdew, K. Pernal, P. Pernot, P. Piecuch, E. Rebolini, L. Reining, P. Romaniello, A. Ruzsinszky, D. Salahub, M. Scheffler, P. Schwerdtfeger, V. N. Staroverov, J. Sun, E. Tellgren, D. J. Tozer, S. Trickey, C. A. Ullrich, A. Vela, G. Vignale, T. A. Wesolowski, X. Xu, and W. Yang, "Dft exchange: Sharing perspectives on the workhorse of quantum chemistry and materials science," *Physical Chemistry Chemical Physics* (2022), 10.1039/d2cp02827a.
- ⁶J. S. Smith, B. T. Nebgen, R. Zubatyuk, N. Lubbers, C. Devereux, K. Barros, S. Tretiak, O. Isayev, and A. E. Roitberg, "Approaching coupled cluster accuracy with a general-purpose neural network potential through transfer learning," *Nature Communications* **10** (2019), 10.1038/s41467-019-10827-4.
- ⁷P. O. Dral, A. Owens, A. Dral, and G. Csányi, "Hierarchical machine learning of potential energy surfaces," *The Journal of Chemical Physics* **152** (2020), 10.1063/5.0006498.
- ⁸S. M. Goodlett, J. M. Turney, and H. F. Schaefer, "Comparison of multifidelity machine learning models for potential energy surfaces," *The Journal of Chemical Physics* **159** (2023), 10.1063/5.0158919.
- ⁹V. Zaverkin, D. Holzmüller, L. Bonferraro, and J. Kästner, "Transfer learning for chemically accurate interatomic neural network potentials," *Physical Chemistry Chemical Physics* **25**, 5383–5396 (2023).
- ¹⁰S. Curtarolo, W. Setyawan, G. L. Hart, M. Jahnatek, R. V. Chepulskii, R. H. Taylor, S. Wang, J. Xue, K. Yang, O. Levy, M. J. Mehl, H. T. Stokes, D. O. Demchenko, and D. Morgan, "Aflow: An automatic framework for high-throughput materials discovery," *Computational Materials Science* **58**, 218–226 (2012).
- ¹¹A. Jain, G. Hautier, C. J. Moore, S. Ping Ong, C. C. Fischer, T. Mueller, K. A. Persson, and G. Ceder, "A high-throughput infrastructure for density functional theory calculations," *Computational Materials Science* **50**, 2295–2310 (2011).
- ¹²S. P. Huber, S. Zoupanos, M. Uhrin, L. Talirz, L. Kahle, R. Häuselmann, D. Gresch, T. Müller, A. V. Yakutovich, C. W. Andersen, F. F. Ramirez, C. S. Adorf, F. Gargiulo, S. Kumbhar, E. Passaro, C. Johnston, A. Merkys, A. Cepellotti, N. Mounet, N. Marzari, B. Kozinsky, and G. Pizzi, "Aida 1.0, a scalable computational infrastructure for automated reproducible workflows and data provenance," *Scientific Data* **7** (2020), 10.1038/s41597-020-00638-4.
- ¹³E. Cancès, A. Levitt, Y. Maday, and C. Yang, "Numerical methods for kohn–sham models: Discretization, algorithms, and error analysis," in *Density Functional Theory: Modeling, Mathematical Analysis, Computational Methods, and Applications* (Springer, 2022) pp. 333–400.
- ¹⁴M. F. Herbst and A. Levitt, "Black-box inhomogeneous preconditioning for self-consistent field iterations in density functional theory," *Journal of Physics: Condensed Matter* (2020), 10.1088/1361-648x/abcdbd.
- ¹⁵M. F. Herbst and A. Levitt, "A robust and efficient line search for self-consistent field iterations," *Journal of Computational Physics* **459**, 111127 (2022).
- ¹⁶E. Cancès, M. F. Herbst, G. Kemlin, A. Levitt, and B. Stamm, "Numerical stability and efficiency of response property calculations in density functional theory," *Letters in Mathematical Physics* **113** (2023),

- 10.1007/s11005-023-01645-3.
- ¹⁷L. Ruddigkeit, R. van Deursen, L. C. Blum, and J.-L. Reymond, "Enumeration of 166 billion organic small molecules in the chemical universe database gdb-17," *Journal of Chemical Information and Modeling* **52**, 2864–2875 (2012), pMID: 23088335, <https://doi.org/10.1021/ci300415d>.
 - ¹⁸R. Ramakrishnan, P. O. Dral, M. Rupp, and O. A. von Lilienfeld, "Quantum chemistry structures and properties of 134 kilo molecules," *Scientific Data* **1** (2014).
 - ¹⁹L. Chanussot*, A. Das*, S. Goyal*, T. Lavril*, M. Shuaibi*, M. Riviere, K. Tran, J. Heras-Domingo, C. Ho, W. Hu, A. Palizhati, A. Sriram, B. Wood, J. Yoon, D. Parikh, C. L. Zitnick, and Z. Ulissi, "Open catalyst 2020 (oc20) dataset and community challenges," *ACS Catalysis* (2021), 10.1021/acscatal.0c04525.
 - ²⁰J. Smith, O. Isayev, and A. Roitberg, "A data set of 20 million calculated off-equilibrium conformations for organic molecules," *Scientific Data* **4** (2017).
 - ²¹E. Bonilla, K. Chai, and C. Williams, "Multi-task gaussian process prediction," in *Advances in neural information processing systems*, edited by J. Platt, D. Koller, Y. Singer, and S. Roweis (MIT Press, Cambridge, Massachusetts, 2008) pp. 153–160.
 - ²²G. Leen, J. Peltonen, and S. Kaski, "Focused multi-task learning in a gaussian process framework," *Machine Learning* **1-2**, 157–182 (2012).
 - ²³G. Pilania, J. Gubernatis, and T. Lookman, "Multi-fidelity machine learning models for accurate bandgap predictions of solids," *Computational Materials Science* **129**, 156–162 (2017).
 - ²⁴R. Batra, G. Pilania, B. Uberuaga, and R. Ramprasad, "Multifidelity information fusion with machine learning: A case study of dopant formation energies in hafnia," *ACS Applied Materials & Inference* **11**, 24906–24918 (2019).
 - ²⁵M. Kennedy and A. O'Hagan, "Predicting the output from a complex computer code when fast approximations are available," *Biometrika* **87**, 1–13 (2000).
 - ²⁶R. Ramakrishnan, P. O. Dral, M. Rupp, and O. A. von Lilienfeld, "Big data meets quantum chemistry approximations: The Δ -machine learning approach," *Journal of Chemical Theory and Computation* **11**, 2087–2096 (2015).
 - ²⁷P. O. Dral, T. Zubatiuk, and B.-X. Xue, "Learning from multiple quantum chemical methods: δ -learning, transfer learning, co-kriging, and beyond," in *Quantum Chemistry in the Age of Machine Learning* (Elsevier, 2023) pp. 491–507.
 - ²⁸V. Vinod, U. Kleinekathöfer, and P. Zaspel, "Optimized multifidelity machine learning for quantum chemistry," (2023), arXiv:2312.05661 [physics.chem-ph].
 - ²⁹G. G. Towell and J. W. Shavlik, "Knowledge-based artificial neural networks," *Artificial Intelligence* **70**, 119–165 (1994).
 - ³⁰L.-M. Fu, "Integration of neural heuristics into knowledge-based inference," in *International 1989 Joint Conference on Neural Networks* (1989) pp. 606 vol.2–.
 - ³¹P. L. Bartlett, A. Montanari, and A. Rakhlin, "Deep learning: a statistical viewpoint," *Acta Numerica* **30**, 87–201 (2021).
 - ³²S. Lotfi, M. Finzi, S. Kapoor, A. Potapczynski, M. Goldblum, and A. G. Wilson, "Pac-bayes compression bounds so tight that they can explain generalization," (2022), arXiv:2211.13609 [cs.LG].
 - ³³C. E. Rasmussen and C. K. I. Williams, *Gaussian Processes for Machine Learning* (the MIT Press, 2006).
 - ³⁴J. Quinonero-Candela and C. Rasmussen, "A unifying view of sparse approximate gaussian process regression," *Journal of Machine Learning Research* **6**, 1939–1959 (2005).
 - ³⁵H. Liu, Y.-S. Ong, X. Shen, and J. Cai, "When gaussian process meets big data: A review of scalable gps," (2018).
 - ³⁶A. G. Wilson, C. Dann, and H. Nickisch, "Thoughts on massively scalable gaussian processes," *CoRR abs/1511.01870* (2015), 1511.01870.
 - ³⁷D. A. Cole, R. B. Christianson, and R. B. Gramacy, "Locally induced gaussian processes for large-scale simulation experiments," *Statistics and Computing* **31**, 1573–1375 (2021).
 - ³⁸P. Abrahamsen, "A review of gaussian random fields and correlation functions," (1997), 10.13140/RG.2.2.23937.20325.
 - ³⁹A. P. Bartók, M. C. Payne, R. Kondor, and G. Csányi, "Gaussian approximation potentials: The accuracy of quantum mechanics, without the electrons," *Physical Review Letters* **104** (2010), 10.1103/physrevlett.104.136403.
 - ⁴⁰A. P. Bartók, R. Kondor, and G. Csányi, "On representing chemical environments," *Physical Review B* **87**, 184115 (2013).
 - ⁴¹A. P. Bartók and G. Csányi, "Gaussian approximation potentials: A brief tutorial introduction," *International Journal of Quantum Chemistry* **115**, 1051–1057 (2015).
 - ⁴²M. Chen, H.-Y. Ko, R. Remsing, M. Andrade, B. Santra, Z. Sun, A. Selloni, R. Car, M. Klein, J. Perdew, and W. Xifan, "Ab initio theory and modeling of water," *Proceedings of the National Academy of Sciences* **114**, 201712499 (2017).
 - ⁴³S. Dasgupta, E. Lambros, J. Perdew, and F. Paesani, "Elevating density functional theory to chemical accuracy for water simulations through a density-corrected many-body formalism," (2021), 10.33774/chemrxiv-2021-hstgf.
 - ⁴⁴M. J. Gillan, D. Alfè, and A. Michaelides, "Perspective: How good is DFT for water?" *The Journal of Chemical Physics* **144**, 130901 (2016), https://pubs.aip.org/aip/jcp/article-pdf/doi/10.1063/1.4944633/13696839/130901_1_online.pdf.
 - ⁴⁵Q. Yu, C. Qu, P. L. Houston, R. Conte, A. Nandi, and J. M. Bowman, "q-aqua: A many-body ccSD(T) water potential, including four-body interactions, demonstrates the quantum nature of water from clusters to the liquid phase," *The Journal of Physical Chemistry Letters* **13**, 5068–5074 (2022), pMID: 35652912.
 - ⁴⁶D. G. A. Smith, L. A. Burns, A. C. Simmonett, R. M. Parrish, M. C. Schieber, R. Galvelis, P. Kraus, H. Kruse, R. Di Remigio, A. Ale-naizan, A. M. James, S. Lehtola, J. P. Misiewicz, M. Scheurer, R. A. Shaw, J. B. Schriber, Y. Xie, Z. L. Glick, D. A. Sirianni, J. S. O'Brien, J. M. Waldrop, A. Kumar, E. G. Hohenstein, B. P. Pritchard, B. R. Brooks, I. Schaefer, Henry F., A. Y. Sokolov, K. Patkowski, I. DePrince, A. Eugene, U. Bozkaya, R. A. King, F. A. Evangelista, J. M. Turney, T. D. Crawford, and C. D. Sherrill, "PSI4 1.4: Open-source software for high-throughput quantum chemistry," *The Journal of Chemical Physics* **152**, 184108 (2020), https://pubs.aip.org/aip/jcp/article-pdf/doi/10.1063/5.0006002/16684807/184108_1_online.pdf.
 - ⁴⁷J. P. Perdew, K. Burke, and M. Ernzerhof, "Generalized gradient approximation made simple," *Phys. Rev. Lett.* **77**, 3865–3868 (1996).
 - ⁴⁸J. Sun, A. Ruzsinszky, and J. P. Perdew, "Strongly constrained and appropriately normed semilocal density functional," *Phys. Rev. Lett.* **115**, 036402 (2015).
 - ⁴⁹A. J. A. Price, K. R. Bryenton, and E. R. Johnson, "Requirements for an accurate dispersion-corrected density functional," *The Journal of Chemical Physics* **154**, 230902 (2021).
 - ⁵⁰X. Huang, B. J. Braams, and J. M. Bowman, "Ab initio potential energy and dipole moment surfaces of (h₂o)₂," *The Journal of Physical Chemistry A* **110**, 445–451 (2006), pMID: 16405316, <https://doi.org/10.1021/jp053583d>.
 - ⁵¹C. Duan, K. Fisher, and H. Kulik, "kefisher98/IP_EA_deltaSCF: Ionization Potential, Electron Affinity, and Delta SCF for Small Organic Molecules," (2023).
 - ⁵²C. Duan, F. Liu, A. Nandy, and H. J. Kulik, "Data-driven approaches can overcome the cost–accuracy trade-off in multireference diagnostics," *Journal of Chemical Theory and Computation* **16**, 4373–4387 (2020).
 - ⁵³C. Duan, S. Chen, M. G. Taylor, F. Liu, and H. J. Kulik, "Machine learning to tame divergent density functional approximations: a new path to consensus materials design principles," *Chem. Sci.* **12**, 13021–13036 (2021).
 - ⁵⁴E. Brémond and C. Adamo, "Seeking for parameter-free double-hybrid functionals: The PBE0-DH model," *The Journal of Chemical Physics* **135**, 024106 (2011).
 - ⁵⁵C. Adamo and V. Barone, "Toward reliable density functional methods without adjustable parameters: The PBE0 model," *J. Chem. Phys.* **110**, 6158–6170 (1999).
 - ⁵⁶C. Lee, W. Yang, and R. G. Parr, "Development of the colle-salvetti correlation-energy formula into a functional of the electron density," *Phys. Rev. B* **37**, 785–789 (1988).
 - ⁵⁷S. De, A. P. Bartók, G. Csányi, and M. Ceriotti, "Comparing molecules and solids across structural and alchemical space," *Physical Chemistry Chemical Physics* **18**, 13754–13769 (2016).
 - ⁵⁸V. Deringer, A. Bartók, N. Bernstein, D. Wilkins, M. Ceriotti, and G. Csányi, "Gaussian process regression for materials and modelling," *Chemical Reviews* **121**, 10073–10041 (2021).

- ⁵⁹F. Musil, A. Grisafi, A. P. Bartók, C. Ortner, G. Csányi, and M. Ceriotti, "Physics-inspired structural representations for molecules and materials," *Chemical Reviews* **121**, 9759–9815 (2021).
- ⁶⁰A. I. J. Forrester and A. J. K. A. Söbester, "Multi-fidelity optimization via surrogate modelling," *Proceedings of Royal Society A* **463**, 3251–3269 (2007).
- ⁶¹A. Reuther, J. Kepner, C. Byun, S. Samsi, W. Arcand, D. Bestor, B. Bergeron, V. Gadepally, M. Houle, M. Hubbell, M. Jones, A. Klein, L. Milechin, J. Mullen, A. Prout, A. Rosa, C. Yee, and P. Michaleas, "Interactive supercomputing on 40,000 cores for machine learning and data analysis," in *2018 IEEE High Performance extreme Computing Conference (HPEC)* (IEEE, 2018) pp. 1–6.
- ⁶²B. Civalleri, D. Presti, R. Dovesi, and A. Savin, "On choosing the best density functional approximation," in *Uncertainty Quantification in Multi-scale Materials Modeling*, edited by M. Springborg (RSC Publishing, 2012) Chap. 6, pp. 168–185.
- ⁶³L. Himanen, M. O. J. Jäger, E. V. Morooka, F. Federici Canova, Y. S. Ranawat, D. Z. Gao, P. Rinke, and A. S. Foster, "DScribe: Library of descriptors for machine learning in materials science," *Computer Physics Communications* **247**, 106949 (2020).

Appendix A: Training Data Cost Model

In our numerical results, we estimate the training cost as

$$\text{model training cost} = \sum_j^m n_j \hat{c}_j$$

where n_j is the number of training systems from the j^{th} level of theory and \hat{c}_j is an estimate of prediction cost for that level of theory. We produce one set of estimates for $\hat{c}_1, \dots, \hat{c}_m$ for the water trimer example and a different set of estimates for the small organic molecules example.

For the water trimers example, we randomly selected ten molecular configurations from our data set as the basis for our cost model. Using Psi4, we computed the 3-b interaction energy at the level of SCAN and CCSD(T) for each configuration. We applied a counterpoise correction to ameliorate basis set superposition error. All computations for the water cost model where performed on physically the same Intel Xeon Platinum 8260 node of MIT SuperCloud (<https://supercloud.mit.edu/systems-and-software>). All computations for a given molecular configuration where performed on the same basis set subbasis set sucure. For this case study, we estimate that a CCSD(T) calculation incurs 37 times the cost of a DFT calculation based on the average prediction time of these methods on our example molecular configurations.

Several configurations in the small organic molecules data set are larger than the water trimer configurations. The median number of electrons in this data set is 40, the minimum is 14, and the maximum is 50. Due to the expense of ionization potential calculations, we base our cost model on energy calculations for ten randomly sampled configurations with 36 electrons. Note that CCSD(T) scales as N^7 where N is the number of electrons in a system while DFT scales as N^3 . Therefore, an estimate of the ratio between the cost of CCSD(T) and the cost of DFT based on 36 electrons will be smaller than the actual ratio for most molecular configurations in our data set. Furthermore, the prediction of ionization potential was performed using ΔCC (delta coupled cluster). Thus, while our

reported results (Fig. 6) estimate that CCSD(T) calculations demand 244 times the expense of DFT, the true ratio between the cost of CCSD(T) and DFT is even larger.

Appendix B: SOAP parameters

To fix reasonable values for parameters required by SOAP (r_{cut} , σ_{atom} , n_{max} , l_{max}), we refer to established conventions as well as experimentation. The cutoff radius, r_{cut} controls the size of each local neighborhood, and a small value may lead to lost geometric insight. Unfortunately, surveys on feature construction^{58,59} hold that a large cutoff radius does not necessarily provide proportionate insight: increasing radii larger than 6–8 Å is rarely if ever useful. Our choice of σ_{atom} also influences our model of each atom’s neighborhood: it determines the lengthscale of the Gaussian shapes located on each of the surrounding atoms. The larger our choice of σ_{atom} , the more chance that Gaussian tails will slip passed the r_{cut} border. Current literature⁵⁸ indicates that the best practice when working with the first three rows of the periodic table is to use $\sigma_{\text{atom}} = 0.3$ Å for systems with hydrogen and $\sigma_{\text{atom}} = 0.5$ Å for systems without. Finally, we choose the parameters n_{max} and l_{max} to control the size of our expansions of the local neighborhoods. Generally⁵⁸, choosing $n_{\text{max}} = 12$ with $l_{\text{max}} = 6$ is sufficient for high accuracy. In practice, the best values for n_{max} and l_{max} will be sensitive to the choice of radial basis set.

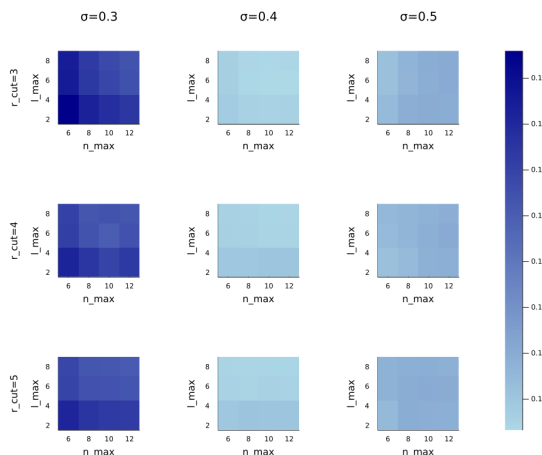


FIG. 7. Example of inference results for a range of SOAP parameters. The colorbar gives the mean absolute error of predictions made for the ionization potential of small organic molecules. Both r_{cut} and σ_{atom} have units of Å.

We selected reasonable candidate values for each SOAP parameter and tested the performance of the resultant features in Gaussian process regression. All features for this work were calculated using the DScribe Python package.⁶³ Fig. 7 shows the mean absolute error (MAE) obtained with different SOAP parameters when GP regression trained with PBE level data is used to predict ionization potential (IP). Tests on CCSD(T) and PBE0 data produced similar results. Our tests include

all combinations of $r_{cut} \in \{3, 4, 5\}$, $\sigma_{atom} \in \{0.3, 0.4, 0.5\}$, $l_{max} \in \{2, 4, 6, 8\}$, and $n_{max} \in \{6, 8, 10, 12\}$. Units for r_{cut} and σ_{atom} are Å. We find that our accuracy is comparable to probabilistic predictions of IP found in literature.⁵⁷ Of the SOAP parameters, the choice of σ_{atom} has the largest impact on predictive performance.

For our numerical experiments in this work, we fix $\sigma_{atom} = 0.4$ Å because this choice demonstrated the best overall performance across our tests. The other parameters are chosen to balance reasonable accuracy and cost. We fix both l_{max} and n_{max} at 8, and for the small organic molecules example, we use $r_{cut} = 4$ Å. For water trimers, we use $r_{cut} = 10$ Å to capture all three component water molecules.

Appendix C: Global Features

When using SOAP to compare two molecular systems, we must make modeling choices to standardize our representation of entire systems. SOAP features are constructed based on the neighborhood of each atom in a system, so challenges arise when two systems contain different numbers of constituent atoms of elements. There are multiple strategies for constructing “global” features to capture entire systems.⁵⁷ The simplest approach is to average the SOAP features for each atom in the system. It is possible the loss of information from averaging may make it challenging to distinguish between the features of similar molecular systems. A variation to this approach averages the local features corresponding to each element contained in a molecular system.⁵⁷ If we wish to compare systems A and B, and system B contains more elements than A, we insert SOAP features corresponding to isolated atoms of those excess elements in the representation of A. This model suggests that an atom of such an element does not interact with the rest of the system. A Regularized

entropy match (REMatch) strategy has also been proposed for constructing global features.⁵⁷ This approach solves a regularized optimization problem to find the match between the sets of local features for each molecular system which maximizes information entropy.

With the same set of small organic molecules which we use to test SOAP parameters, we investigate how well the global features constructed by different approaches agree. For pairs of molecules, we construct global features using each of the three approaches outlined in the previous paragraph. We represent difference between each pair by squaring an inner product of their features. This procedure is the same as using a polynomial kernel of degree 2. By comparing the output of the kernel for different featurization strategies, we determine whether the strategies generally agree about which molecules are similar.

Fig. 8 shows the correlation in kernel outputs corresponding to each pair of molecules for different global featurization strategies. Consistently, in our tests, we find strong correlation (Pearson’s coefficient > 0.99) between the REMatch features and features computed by averaging all local representations. These two strategies are also both positively correlated with the “Average by Species” approach which produces an averaged feature for each element in the system and inserts isolated atoms to represent elements not included in the system, but these correlations are not as strong as that between the REMatch and totally averaged features. We may see this result because the REMatch and totally averaged features share the same dimension, n , whereas features that are constructed by species specific averaging have dimension of $2n$ to $4n$ in the cases we considered. Because averaging features is much more computationally efficient than constructing REMatch features, we use this approach in our numerical experiments.

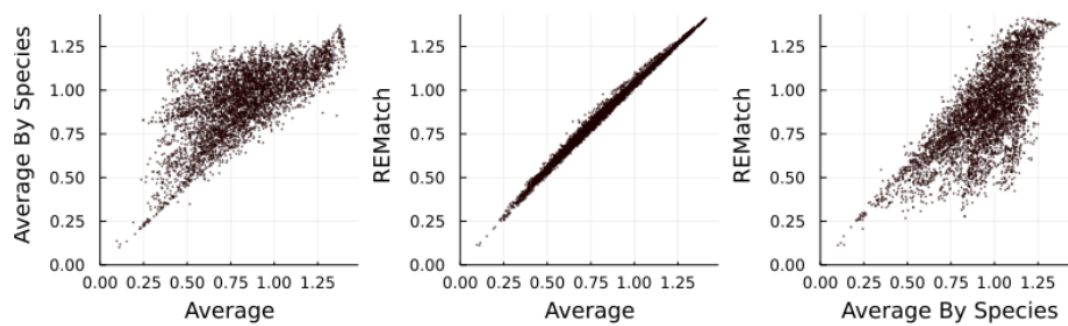


FIG. 8. Correlation between different methods of constructing global features when calculating the distance between molecule pairs.⁵⁷